

Large and stable band gaps in spin-polarized graphene antidot lattices

Mads L. Trolle,^{1,*} Ulrik S. Møller,¹ and Thomas G. Pedersen^{1,2}

¹*Department of Physics and Nanotechnology, Aalborg University, Skjernvej 4A, DK-9220 Aalborg East, Denmark*

²*Center for Nanostructured Graphene (CNG), Aalborg University, DK-9220 Aalborg East, Denmark*

(Received 7 June 2013; published 15 November 2013)

Introducing a periodic array of holes, i.e., an antidot lattice, in a graphene sheet has been suggested as a route towards the tantalizing objective of “opening the gap” in this otherwise zero-gap semiconductor. Combining density-functional and mean-field Hubbard tight-binding methods, we study the effect of spin polarization on graphene antidot lattices (GALs). Focusing on GALs with extended zigzag edges, we systematically investigate the geometry dependence of spin polarization, electronic structure, and band gaps. A scaling law for the band gap is established, demonstrating marked deviations from that of circular holes without spin polarization. Furthermore, we estimate the robustness of the magnetic ordering against raised temperature and doping and, finally, consider how the optical properties are modified by spin polarization. Our results demonstrate that large, stable band gaps are expected for a range of geometries.

DOI: [10.1103/PhysRevB.88.195418](https://doi.org/10.1103/PhysRevB.88.195418)

PACS number(s): 73.22.Pr, 75.70.-i, 75.75.-c, 78.67.-n

I. INTRODUCTION

Graphene is today one of the most intensively studied novel materials with promising applications within, e.g., flexible two-dimensional electronics or transistor technology.¹ These capabilities are facilitated by the extraordinary room-temperature electron mobility² in excess of $10^5 \text{ cm}^2 \text{ V}^{-1} \text{ s}^{-1}$ of exfoliated graphene. Importantly, graphene can now be synthesized on wafer scale using chemical vapor deposition techniques.³ However, one of the shortcomings of graphene remains its vanishing band gap, limiting applications as a substitute for the materials used today in semiconductor devices. Several strategies, including confinement in nanoribbons⁴⁻⁶ and biased bilayer structures,^{7,8} have been suggested with the ultimate goal of “opening the gap.” Also, periodic arrays of holes, so-called graphene antidot lattices (GALs), have been proposed as a route towards large-scale gapped graphene.⁹ Since their proposal, the physical properties of GALs have been the subject of intense theoretical research, focusing on, e.g., their electronic structure,¹⁰⁻²⁰ optical properties,²¹ or transport capabilities.²²⁻²⁶ Many of these calculations are, with some exceptions,^{11,14,15,17-20} performed neglecting effects of spin polarization, even though this phenomenon has been demonstrated in recent experiments on zigzag graphene nanoribbons (ZGNRs) using scanning tunneling spectroscopic methods.²⁷ Quite generally, extended regions of zigzag edges in graphene nanostructures favor spin polarization. This is readily observed by inclusion of a mean-field Hubbard interaction in a tight-binding scheme, which modifies the electronic structure drastically near the band gap.²⁸⁻³¹ In fact, neglecting spin polarization, ZGNRs are semimetals characterized by two degenerate, dispersionless bands at the Fermi level, developing a band gap of several hundred meV with inclusion of a Hubbard-type interaction—a trend also supported by more complex *ab initio* approaches based on, for example, density-functional theory,^{5,6} configuration interaction,³² density-matrix renormalization-group methods,³³ or quantum Monte Carlo simulations.^{34,35} While the existence of band gaps in GALs with no spin polarization can be reasoned from band-folding arguments based on the periodicity of the superlattice,¹⁰ band gaps induced by spin-polarized GAL

zigzag edges cannot be understood by such simple considerations, requiring instead atomistic calculations similar to the ones mentioned above.

The near-perfect zigzag edges necessary for supporting spin polarization in the aforementioned experiment can be attributed to the production of the ZGNRs by “unzipping” carbon nanotubes. While any edges realistically produced in GALs, usually fabricated by lithographic methods,³⁶⁻³⁹ are considerably more disordered, postprocess annealing has been shown to reconstruct disordered edges of single holes into zigzag or armchair shapes,^{40,41} making extended regions of these two edge types experimentally feasible. Additionally, very recent experimental results suggest that fabrication of GALs with hexagonal holes of preferably zigzag character may be possible by anisotropic edging techniques.⁴² Furthermore, magnetic force microscopy has revealed spin-polarized zigzag edges in hexagonal GALs on the 100 nm scale fabricated using a nanoporous alumina template.⁴³ Thus, with other GAL fabrication techniques approaching the 10 nm regime,^{36,37} special attention towards the theoretical understanding of the magnetic properties and resulting band-gap modulations of antidots with extended zigzag edges is warranted.

GALs containing a dissimilar number of atoms in the *A* and *B* sublattices are by Lieb’s theorem⁴⁴ predicted to display a net magnetic moment in their ground state, and extensive work has been done on the microscopic modeling of these ferromagnetic systems.^{15,19,45} In addition, GALs with an identical number of *A* and *B* atoms are reported to display local spin polarization at zigzag edges, even though their net magnetic moment vanishes.^{15,17} However, this occurs only for larger holes with smaller ones remaining completely unpolarized.⁴⁵ To our knowledge, no systematic study has been performed on the antiferromagnetic spin ordering of GALs with hexagonal holes of varying dimensions, and we therefore here consider spin polarization in two families of GALs with hexagonal holes in a triangular lattice. These antidots might be envisaged as particularly well ordered reconstructions of roughly circular holes into ones dominated by zigzag edges. Also, this is exactly the structure used by Shimizu *et al.* to interpret their experimental results; see Fig. 1. We follow the nomenclature of Ref. 13 and denote such lattices, for which all lattice vectors are

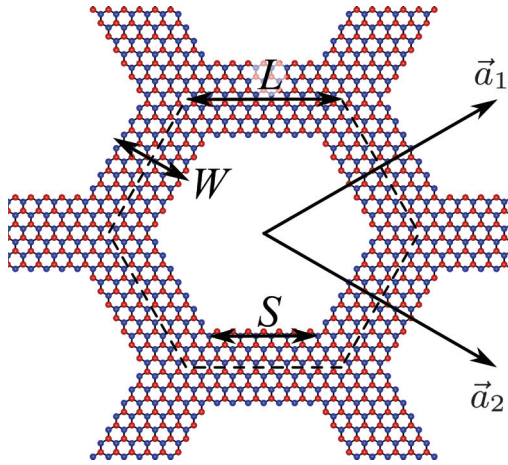


FIG. 1. (Color online) Excerpt of a triangular GAL with hexagonal holes. W , S , and L represent the subribbon width, edge length, and unit-cell size, respectively, whereas \vec{a}_1 and \vec{a}_2 are GAL lattice vectors parallel to carbon-carbon bonds. The edges are zigzags of alternating carbon atoms from the A and B sublattices illustrated by blue and red atoms, respectively. The dashed line indicates the unit cell.

oriented parallel to carbon-carbon bonds as “triangular” GALs. Calculations neglecting spin-polarization have predicted these structures to be semiconducting with band gaps decreasing with increasing unit cell size (i.e., with holes constituting a smaller fraction of the unit cell).^{11,23} However, upon rotating the holes further by $\pi/6$ around the hole center axes, making the angle between GAL lattice vector and carbon-carbon bond $\pi/6$, only structures with a unit cell edge length of $(3n + 3)a_0$ (n an arbitrary integer and a_0 the graphene lattice constant) were found to retain a sizable band gap.^{10,13} Following Ref. 13, we term these “rotated triangular” GALs, and the question remains to what extent this simple rule for band-gap opening transfers to the spin-polarized case.

In this paper, we seek to identify the geometrical requirements for GALs supporting spin polarization, and furthermore consider the effects on the electronic structure of GALs with unit cells and holes on the nanometer scale. The limits of small and large holes resemble spin-unpolarized graphene and spin-polarized ZGNRs, respectively, and we therefore aim to identify the critical size for the transition. Hence, the minimum edge length required will be identified for both lattice types. We seek to identify to what extent simple rules for band-gap opening found neglecting spin magnetization remain valid in the spin-polarized cases. Additionally, we consider the stability of the polarization with respect to raised temperatures and chemical doping and finally consider the modulation of the linear optical spectra due to inclusion of spin. The applied theoretical frameworks will be presented in the following section. Then, results for the magnitude and stability of the spin polarization and band gaps are shown in Sec. III along with the optical response. Finally, conclusions are given in Sec. IV.

II. METHODS

Hexagonal graphene antidots in a triangular lattice can be characterized by a unit-cell edge length parameter L and

hole edge length S , both in units of a_0 . These are defined as the number of zigzags along the edges shown in Fig. 1 for triangular GALs, agreeing with the nomenclature of, e.g., Refs. 13, 23, and 45, making the illustrated GAL an $\{L = 10, S = 7\}$ structure. Alternatively, the structure can be envisaged as consisting of interconnected zigzag subribbons of length S and width $W = L - S$, the latter indicating the number of armchairs, each of length $\sqrt{3}a_0$, connecting the two subribbon edges indicated in Fig. 1. Hence, the limiting case of large S should approach the case of infinite ZGNRs of width W , whereas the case of small S approaches pristine graphene with no spin polarization. This means that a transition region in S and L must exist where the ground state evolves from having a vanishing spin polarization to having a finite one.

We apply a model based on density-functional theory (DFT) in the local spin-density approximation (LSDA) as implemented in the SIESTA package⁴⁶ to investigate structures with small unit cells. We verify its agreement with a much simpler mean-field Hubbard tight-binding model, and use this to consider structures with unit cells of several thousand atoms beyond the scope of DFT. Here, characteristic properties such as optical gaps and spin polarization become asymptotic, allowing for extrapolation to the behavior of even larger systems.

A. Density-functional theory model

In the DFT model, all dangling bonds are hydrogen terminated, removing them from the band gap. A double- ζ basis, with an extra polarized term and Troullier-Martins pseudopotentials⁴⁷ with only $2s$ and $2p$ electrons treated as valence for carbon, are used. Exchange and correlation is handled in the Perdew-Zunger parametrization.⁴⁸ A modest $2 \times 2 \times 1$ Monkhorst-Pack k grid was found to be sufficient for k -space integration due to the relatively flat bands and semiconducting nature of the GALs investigated, except for the specific case of $S = 5$ where the spin polarization was found to vanish with increasing k -grid sampling, making an $8 \times 8 \times 1$ grid necessary. Additionally, several hundred iterations were required to fully converge the spin densities of $S = 5$ structures, whereas only tens of iterations were necessary with $S \neq 5$. A reciprocal wave vector cutoff of 150 Ry was found to be sufficient. Unrelaxed structures with ideal carbon-carbon and hydrogen-carbon bond lengths respectively $2.46/\sqrt{3}$ Å and 1.09 Å were used.

B. Hubbard tight-binding model

Generally, the out-of-plane π -electron system of planar conjugated carbon structures decouples from the in-plane σ system, and since the π electrons govern optical and electronic properties of the states in the vicinity of the Fermi level we include these only in the Hubbard tight-binding (HTB) treatment. In the mean-field (Hartree-Fock) approximation, the Hubbard Hamiltonian becomes

$$\hat{H} = \sum_{i,j,\sigma} t_{ij} \hat{c}_{i\sigma}^\dagger \hat{c}_{j\sigma} + U \sum_{i,\sigma} \hat{n}_{i\sigma} (\hat{n}_{i,-\sigma}), \quad (1)$$

where $\hat{c}_{i\sigma}$ and $\hat{c}_{i\sigma}^\dagger$ are, respectively, annihilation and creation operators of electrons in atomic π orbitals at lattice site

i with spin σ . t_{ij} is the tight-binding hopping parameter between sites i and j , whereas U is the Hubbard interaction parameter coupling the $-\sigma$ spin density $\langle \hat{n}_{i,-\sigma} \rangle$ to the σ density through the occupation number operator $\hat{n}_{i\sigma} = \hat{c}_{i\sigma}^\dagger \hat{c}_{i\sigma}$. In the following, we take $U = 2.0$ eV and include up to third-nearest-neighbor interactions using hopping integrals $t_1 = -2.7$ eV, $t_2 = -0.2$ eV, and $t_3 = -0.18$ eV. These Hubbard and tight-binding parameters were previously shown to convincingly reproduce DFT LSDA results for ZGNRs,⁴⁹ and we here confirm that they are transferable to GAL structures by comparison with our SIESTA model. Long-range Coulomb interaction, treatable in the extended Hubbard scheme, has been shown to map onto the purely local Hubbard model used here by introduction of an effective and filling-independent (at least in the doping range considered here) Hubbard parameter.⁵⁰ Thus, we expect the HTB model to generate results comparable to DFT LSDA results for large GAL structures.

Using the HTB Hamiltonian, the initially antiferromagnetic densities are iterated to self-consistency. We note that quantum fluctuations arising from electron correlation effects not included in mean-field models can be important in strongly correlated graphene systems. However, good agreement between the quantum Monte Carlo and mean-field approaches to the Hubbard model has been demonstrated for graphene nanoribbons of moderate width $W > 3$ and Hubbard parameters comparable in magnitude to the nearest-neighbor hopping integral.^{34,35} In particular, an almost quantitative agreement for low-energy excitation features was found.³⁴ Thus, since the Hubbard U applied by us belongs to this range and since we mainly use the Hubbard model for large structures, we expect the mean-field approach to be a good approximation.

III. RESULTS AND DISCUSSION

As already discussed, at sufficiently large S the GALs under investigation are expected to display antiferromagnetic behavior akin to what is observed for ZGNRs. This is indeed what we find, with an example shown in Fig. 2 where antiferromagnetic ordering is seen with respect to the A and B sublattices indicated by blue and red atoms in Fig. 1. At the armchair corners joining two oppositely polarized edges, polarization is strongly suppressed, while a maximum is found at the edge center atom. All spin-polarized GALs investigated here follow this general trend, and below we present a systematic investigation of the influence of the dimensions (i.e., W and S) on spin polarization and band gaps. However, we first make some general comments on the modulation of the electronic structure upon including spin polarization in the problem.

In Fig. 3, we display the density of states calculated for each spin projected onto the edge atoms of the A sublattice $P_A(E, \sigma)$ for a $W = 2$ structure and a few edge lengths. Note that the same quantity for the B sublattice is found by simply interchanging the spin index due to the antiferromagnetic symmetry of the sublattices, as can be readily seen from the spin-density difference in Fig. 2. By inspection of the electron wave function, the edge localization of the states nearest the band gap was confirmed, and it is clearly observed by comparison with the total density of states $D(E)$ that these

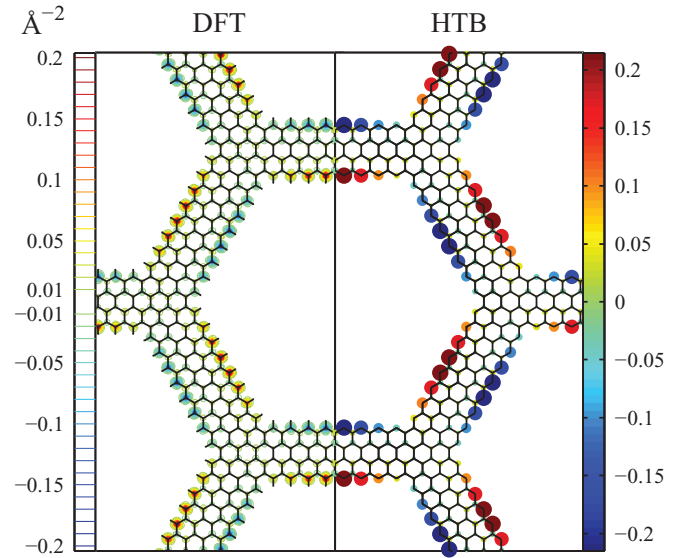


FIG. 2. (Color online) Spin polarization of $\{W = 2, S = 8\}$ triangular GAL, comparing the z -integrated DFT density with the on-site HTB density. Note that the DFT density is plotted as a contour plot, with contour lines at values shown in the left bar, while the HTB model is a scatter plot, with dot sizes and colors indicating the on-site Hubbard spin-density difference.

dominate in this energy region. Additionally, at $S > 5$ the edge states become spin polarized with a clear difference in up and down densities. Interestingly, the opposite polarization is observed for edge states just above the band gap, hinting at why spin polarization is suppressed by occupying the lowest conduction-band states by, e.g., doping. Furthermore, only states near the band gap are polarized, while states with significant weight near the edges extending further into the valence-/conduction-band range remain unpolarized. This trend can be seen by comparing the weakly polarized [i.e., small difference between $P_A(E, \uparrow)$ and $P_A(E, \downarrow)$] peaks near -0.35 eV for the $S = 8$ structure in Fig. 3 with the strongly polarized peaks near -0.18 eV, where the projected density of states is almost exclusively spin down.

In order to systematically quantify the degree of spin-polarization in the investigated GALs, we use “maximum spin polarization.” In general, this value is simply the absolute spin-density difference (on-site occupation for the HTB model and out-of-plane integrated density for the DFT model) found at the middle of (any) subribbon edge.

A. Spin polarization and band gap

In Fig. 4, we consider the scaling of the maximum spin polarization (lower panel) and band gap (upper panel) with edge length S and width W . We find a characteristic length of $S = 5$ above which structures of all widths W are spin polarized. Both DFT and HTB results display this behavior, which can simply be interpreted as a competition between the energy gain due to polarization of the zigzag subribbons and the energy penalty of polarizing the armchair corners. Given the good agreement between DFT and HTB results, and the fact that they both predict the same characteristic length, we are confident that the HTB model faithfully

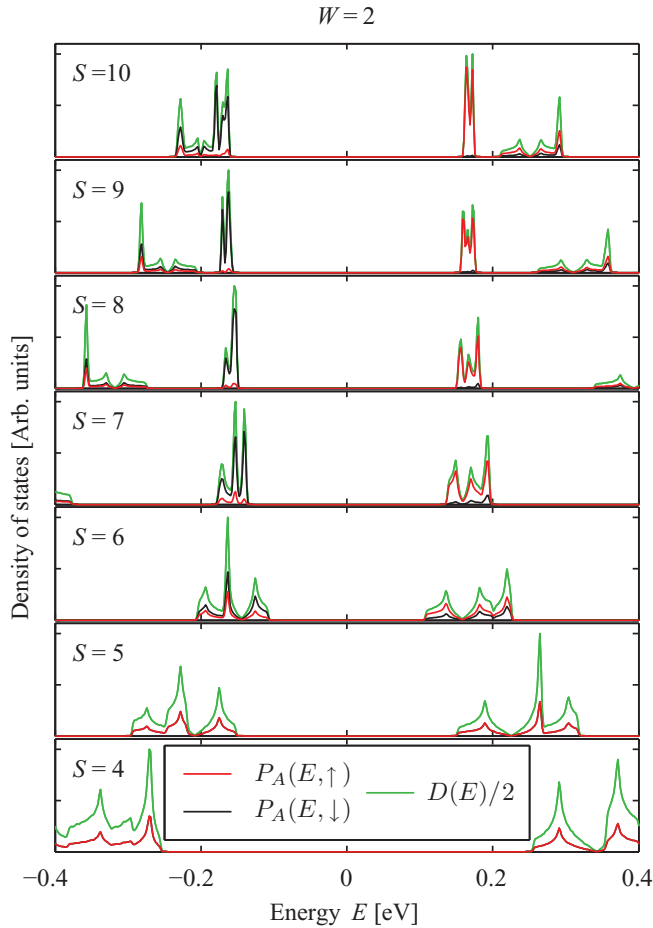


FIG. 3. (Color online) Density of states calculated using our HTB model for a few triangular GALs, with subribbon width $W = 2$ and varying edge length S , projected onto the edge atoms of the A sublattice (red and black curves) in addition to the total density of states (green curve).

reproduces DFT results also for larger structures. We note that Ref. 17 reports DFT calculations showing a weakly spin-polarized $S = 5$ structure, in contrast to our findings. However, their calculations were performed using a $2 \times 2 \times 1$ k -point sampling, which we found insufficient, as discussed previously.

As demonstrated in the upper panel of Fig. 4, the onset of spin polarization coincides with a dramatic opening of the band gap in comparison to the unpolarized case for $S > 5$. Hence, spin polarization breaks the tendency of decreasing band gap with S and leads to gaps tending asymptotically to values resembling those of spin-polarized infinite ZGNRs of similar widths W reported in, e.g., Refs. 5 and 49. Thus, the band gaps predicted by us are in the same range as those generally considered realistic for nanostructured graphene systems in DFT studies, and the HTB model ensures the correct limiting behavior for $L/W \gg 1$. Conversely, in calculations excluding Hubbard interaction [i.e., setting $U = 0$ eV in Eq. (1)] the band gap decreases monotonically with increasing S , although with weak oscillations at $S > 10$ due to confinement effects depending on edge lengths. Hence, the band gaps of even relatively large GALs are expected to be on the order of hundreds of meV, as opposed to our previous predictions for

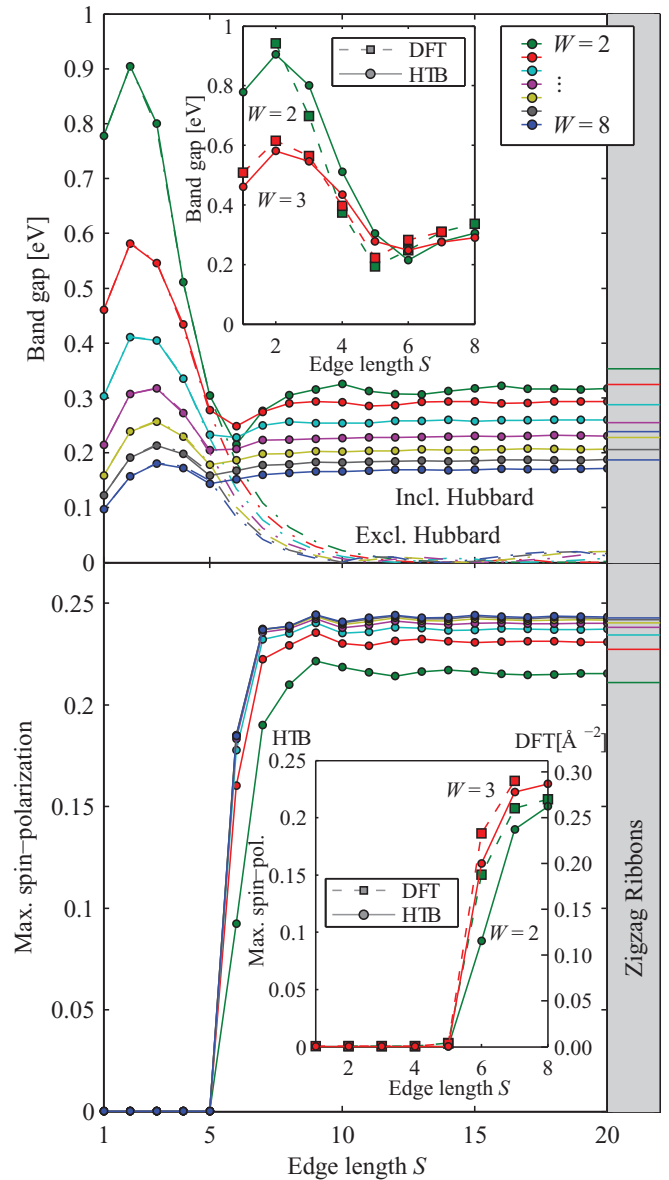


FIG. 4. (Color online) Band gap (top) and maximum spin polarization (bottom) of triangular GALs of varying dimensions calculated using the Hubbard model. The band gap is seen to vanish with increasing hole size for fixed W if spin is neglected (dash-dotted lines). However, the Hubbard interaction term introduces a finite band gap resembling those of ZGNRs, shown in the shaded region, for large hole sizes. A band-gap increase is seen at edge lengths S larger than 5 for all structures, matching the onset of spin polarization. DFT results are shown in the insets, where the onset of spin polarization is in full agreement with the HTB model. Additionally, the DFT and HTB band gaps are in reasonable agreement, with the position of the band-gap minimum near $S = 5$ reproduced by both methods.

circular holes without spin polarization,⁹ enforcing the idea of utilizing GALs in semiconductor devices.

For circular, unpolarized holes, a simple scaling law was proposed by Pedersen *et al.*⁹ for the band gap $E_g \approx \alpha N_{\text{rem}}^{1/2}/N_{\text{tot}}$, with N_{rem} indicating the number of atoms removed from a unit cell that would otherwise contain N_{tot} atoms and α a fitting parameter. For the present case, in which

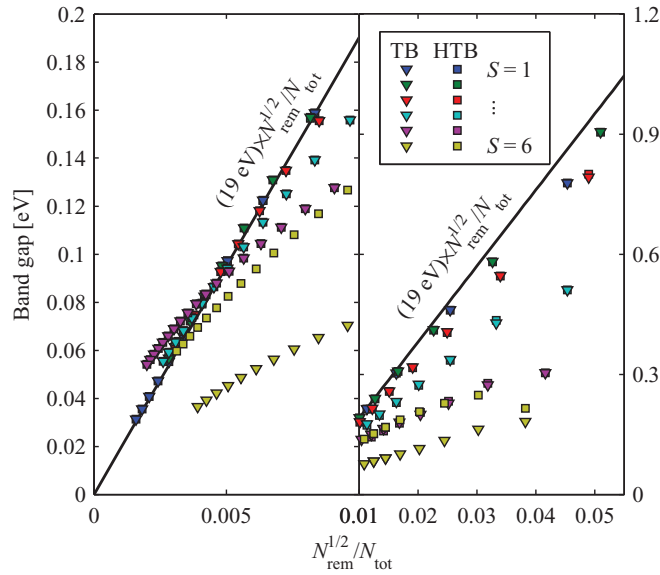


FIG. 5. (Color online) Comparison of the tight-binding models including (HTB) and neglecting (TB) Hubbard interaction with scaling rule of Ref. 9 (full black line).

$N_{\text{rem}}^{1/2}/N_{\text{tot}} = S/[\sqrt{6}(W + S)^2]$, we note that the band-gap dependency follows such a simple scaling law only for the smallest holes as demonstrated in Fig. 5. In the original work, $\alpha = 25$ eV was found by fitting to tight-binding band gaps for circular holes, whereas α was set to values ranging from ~ 4 to 25 eV by Liu *et al.*,¹⁵ allowing fits to triangular and rhombus-shaped holes. Hence, this law is widely used as a benchmark for comparing band gaps in GALs of varying geometries. For very small holes, $S = \{1, 2\}$, a good fit can be made to our results using $\alpha = 19$ eV (shown as the black line of Fig. 5) for a wide range of unit-cell sizes L . However, with edge lengths $S > 2$ this tendency is broken. By adjusting the value of α and introducing corrections similar to those in Ref. 15 reasonable fits in a large range of L can still be obtained for $2 < S < 6$. At $S > 5$, spin polarization sets in which increases the band gap, causing a nonlinear behavior in $N_{\text{rem}}^{1/2}/N_{\text{tot}}$ clearly seen near $N_{\text{rem}}^{1/2}/N_{\text{tot}} = 0.04$ for the $S = 6$ structure. Hence, for structures with larger holes ($S > 5$), significant deviations between the simple scaling law and our results are found, becoming increasingly severe with hole size. In the limit of very small holes, however, the simple scaling law does seem to hold, as is seen in the left panel of Fig. 5. In this regime, inclusion of spin polarization actually improves the agreement between the scaling law and the tight-binding models. For the structures produced experimentally by Shimizu *et al.*,⁴³ we can estimate $N_{\text{rem}}^{1/2}/N_{\text{tot}} \sim 10^{-3}$ based on the atomic force microscopy images presented in that letter. Other fabrication techniques, such as block copolymer methods,³⁶ allow $N_{\text{rem}}^{1/2}/N_{\text{tot}} \sim 0.01$. Hence, experimentally available structures are well within the regime considered here. However, we do not expect structures with extended zigzag edges to follow the above scaling law. Rather, band gaps in such structures must approach those of the nanoribbons comprising the structure. For example, the case of large S and modest W is better described by the scaling rule presented

in Ref. 5: $E_g \approx (9.33 \text{ eV } \text{\AA})/(w + 15.0 \text{ \AA})$ for band gaps in spin-polarized, infinite graphene zigzag nanoribbons of width $w = W\sqrt{3}a_0$.

In Ref. 15, results for rhombus-shaped holes in a triangular lattice with zigzag edges calculated using a nearest-neighbor Hubbard tight-binding model were reported. There, a band gap increase from ~ 250 to ~ 500 meV with hole side length varying from $5a_0$ to $10a_0$ for constant unit-cell side length $14a_0$ was found. The opposite holds true for increasing unit-cell size (between $10a_0$ and $15a_0$) with constant hole side length ($5a_0$). Additionally, they found the ground state to be antiferromagnetically spin polarized. These results agree closely with ours, even though their calculations are performed for rhombus-shaped holes.

Hence, the existence of a relatively short edge length over which spin polarization becomes a dominating effect suggests that this may indeed not be negligible in experimentally feasible systems. The question remains, however, how robust this magnetic ordering is against, e.g., temperature increase and doping levels, as will be discussed below.

B. Band-gap rules for rotated holes

In Ref. 13, Petersen *et al.* formulated a semiempirical rule stating that only every third rotated triangular GAL displays a significant band gap, requiring $L = 3n + 3$, where n is an integer and the unit-cell size L for the rotated structure is defined as the number of zigzags along the unit-cell edge indicated in Fig. 6. Similarly, Ouyang *et al.*¹⁶ observed an alternating semiconducting/metallic behavior of triangular GALs with hole separation distance. Recently, Liu *et al.*¹⁰ demonstrated that these results are particular realizations of

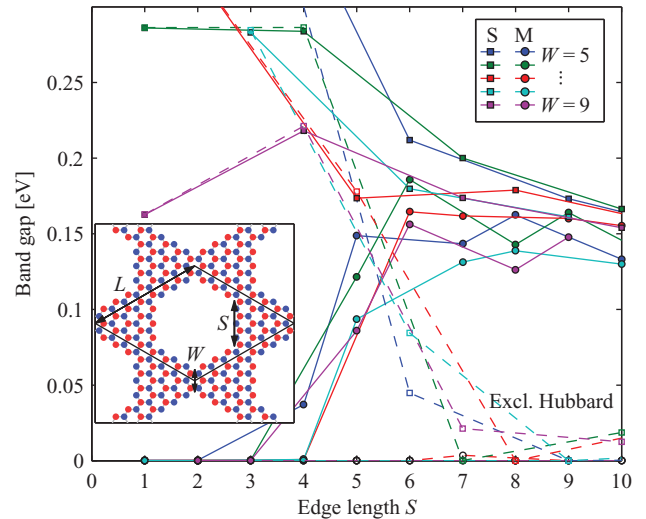


FIG. 6. (Color online) Band gaps of a few rotated triangular GALs calculated using the HTB model. Structures which are metallic in the absence of Hubbard interaction are denoted by circles as indicated by the “M” in the legend, whereas squares indicate semiconducting structures, denoted by “S” in the legend. The full and dashed lines indicate results including and excluding Hubbard interaction, respectively. The inset illustrates the unit cell (full black line) of the rotated triangular structure, together with the side length parameters S and L , in addition to a width parameter $W = L - 2S$.

a universal rule governing band-gap opening in all triangular superlattices spanned by integer combinations of graphene lattice vectors. We have considered a range of rotated triangular unit cells, both including and excluding Hubbard interaction, and verify this rule in the latter case. However, upon including Hubbard interaction the rotated triangular structures are found to be antiferromagnetically spin polarized, breaking the A - B sublattice symmetry. This, in turn, induces a band gap comparable to those in Fig. 4.

This is exemplified by the results in Fig. 6. No common threshold edge length S , above which all structures are spin polarized, could be found for these structures. Instead this threshold depends on the width parameter W , in contrast to what is observed in Fig. 4. The spin polarization (not shown) increases abruptly exactly at edge lengths where the band gaps including and excluding Hubbard interaction diverge, as in Fig. 4. Band-gap openings similar to the ones observed here are expected for other structures, which is why care should be taken in generalizing the aforementioned band-gap rules to any structure containing extended, possibly spin-polarized zigzag edges.

C. Doping and temperature effects

Band gaps induced by spin polarization in ZGNRs are known to close by doping.⁵¹ Here, we consider to what extent a similar effect is found for the antiferromagnetic ordering of GALs. We investigate the effects of both thermal excitations and carriers injected by dopants or charge reservoirs such as a metallic substrate. Thermal excitations are included by applying finite-temperature Fermi-Dirac statistics when calculating the electron density. Thus, the bottom conduction bands displaying a spin polarization opposite that of the top valence bands contribute to the charge density, causing an overall reduction in spin polarization. This, in turn, causes a reduction of the band gap which allows the thermal excitation of further conduction-band electrons reducing the band gap even more. The results are shown in Fig. 7 for structures of the type presented in Fig. 1, where it is clearly observed how all GALs depolarize near 1000 K, regardless of band gap. We note that other thermal mechanisms exist which may disrupt the magnetic order in GALs well below 1000 K, e.g., lattice distortions or quantum fluctuation effects. Also, from statistical mechanics the Mermin-Wagner theorem states that phase transitions breaking extended symmetries cannot occur at any finite temperature in one- and two-dimensional systems with sufficiently short-ranged interactions.^{52,53} In fact, this excludes the possibility of spontaneous formation of both ferromagnetic and anti-ferromagnetic phases in systems governed by a purely local Hubbard model.⁵⁴ *Ab initio* calculations suggest, however, that upon including long-range Coulomb interaction (as in, e.g., DFT models) ordered magnetic phases are indeed realistic well above room temperature in related systems such as graphene nanoribbons⁵⁵ or point defects.^{56,57} Here, however, we have analyzed the important case of thermal carrier injection on antiferromagnetically prepared ground states by equilibrium statistics using the Hubbard model as a rough guide, and find this not to close the induced band gaps at room temperature. On a final note, we emphasize that models treating Coulomb interaction accurately may be

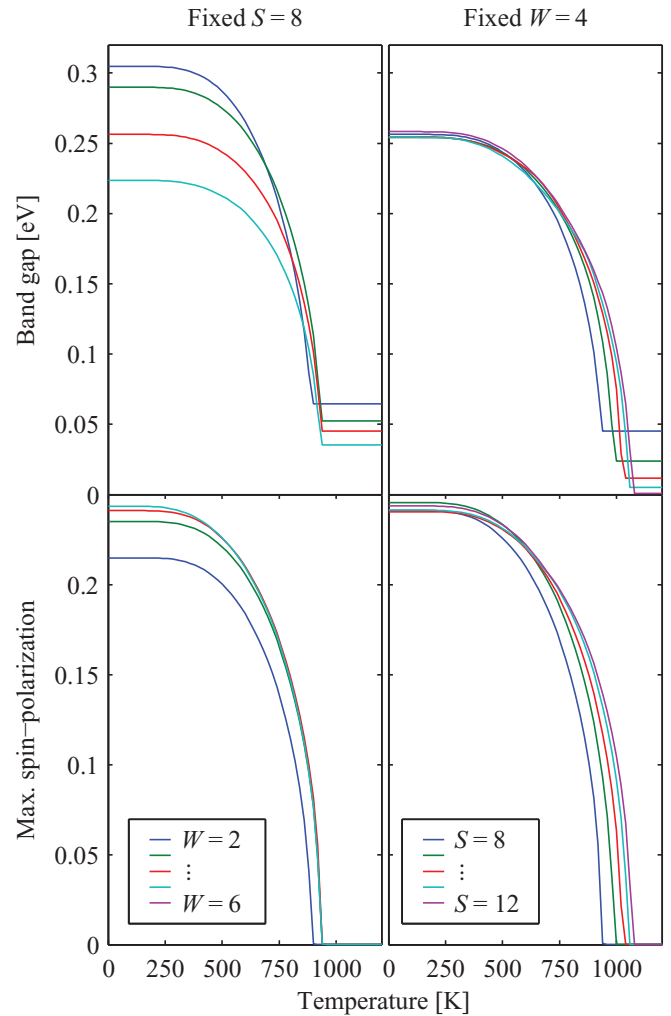


FIG. 7. (Color online) Band gap and maximum spin polarization of several triangular GALs at varying temperatures calculated using the HTB model. All species tend to depolarize at temperatures larger than approximately 1000 K, regardless of band gap.

necessary to capture the correct temperature dependence of spin polarization in GALs.

Charge carriers injected (at zero temperature) by, e.g., chemical doping can be treated by adjusting the Fermi level into the conduction-band range at an energy yielding an electron number satisfying the chosen doping level, and the results are displayed in Fig. 8. A clear spin depolarization (and hence decreasing band gap) is observed with increasing number of injected electrons. However, for all ribbons a complete depolarization is observed only at relatively high doping levels, close to 1% increase in electrons per unit cell relative to the intrinsic case. Additionally, all GALs appear increasingly sensitive towards doping with increasing W for constant S . This trend can be understood by noting that the number of edge states is proportional to the edge length S , while the number of doping electrons scales with the number of atoms per unit cell (the doping levels are given in percentages of electrons per unit cell) and hence W . Thus, with increasing W and constant S , the doping level per edge state increases. These edge states are energetically located near the conduction-band minimum with spin polarization

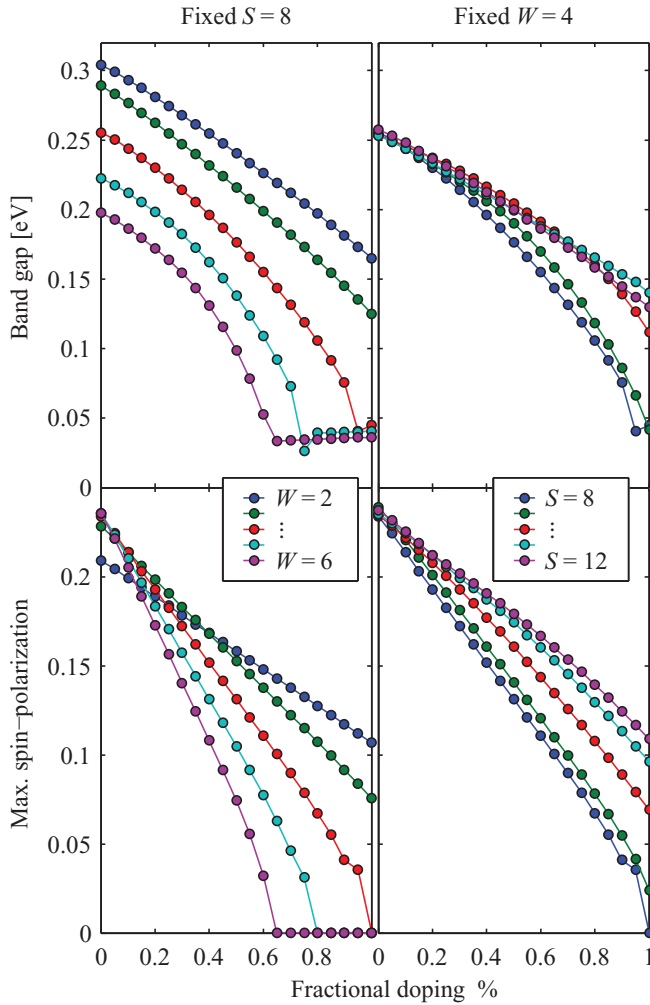


FIG. 8. (Color online) Band gap and maximum spin polarization of triangular GALs calculated for various doping levels and structure parameters using the HTB model.

antisymmetric to those of the top valence bands, as discussed previously. It follows that occupation of conduction-band edge states causes an overall spin depolarization. We note that in order to accurately model chemical doping at the highest levels considered here, modulations of the band structure should be taken into account,^{58,59} but this complication is ignored here.

D. Linear optical response

Noting the dramatic effects of spin polarization on the band structure near the band gap, we expect substantial modifications of the optical properties of GALs relative to results calculated neglecting Hubbard interaction, e.g., in Ref. 21. We calculate the optical conductivity using the method described in that paper both including and excluding Hubbard interaction for triangular GALs of $W = 2$, and present the results in Fig. 9. The optical spectra for small holes ($S < 5$) are nearly identical regardless of the Hubbard interaction; however, for larger structures ($S > 5$) dramatic modulations in the optical spectra are found. Most notably, the band-edge transition is blueshifted by several hundred meV due to spin polarization, as might be expected due to the changing band

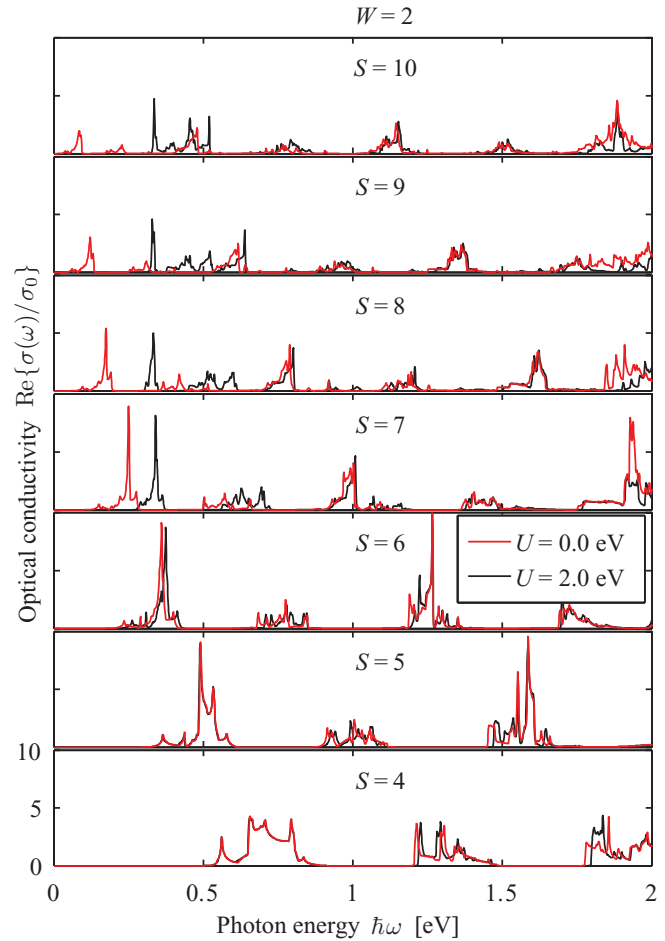


FIG. 9. (Color online) Optical response of various triangular $W = 2$ GALs from the HTB model in units of the static conductivity of graphene, $\sigma_0 = e^2/(4\hbar)$.

gap. Additionally, the peak shapes tend to differ slightly for larger holes due to the flattening of the edge-state bands upon inclusion of Hubbard interaction. We note that the results presented here are calculated neglecting complications such as excitonic effects or electron-phonon interaction. While such phenomena are expected to affect the optical response to some extent, the single-particle spectra remain an important first approximation, demonstrating the impact of spin polarization on a readily measurable quantity. An equally dramatic impact on the transport properties of GALs with hole edge lengths larger than $5a_0$ might also be expected.

IV. CONCLUSION

The ground-state electron densities of graphene antidot structures with hexagonal holes in a triangular lattice display antiferromagnetic spin polarization similarly to what is observed for graphene zigzag nanoribbons, but only for hole sizes with an edge length larger than five graphene lattice constants. This has a large effect on the band structure near the Fermi level, with a substantial band gap increase of several hundred meV. Also, structures with a rotated hole, previously reported to display an alternating semiconducting/metallic behavior with increasing unit-cell size, were found to be purely

semiconducting with the inclusion of spin polarization and modest hole sizes. For antidots with extended zigzag edges, this result questions the validity of simple scaling laws and rules for band-gap opening based on calculations neglecting spin polarization.

The states near the band gap are localized at the graphene edges and display a strong spin polarization, with the states just above or below the Fermi level being oppositely polarized. Thus, with increasing temperature and doping, electrons occupy edge bands on both sides of the band gap. This results in a net reduction of the spin polarization and consequently reduced band gaps. However, the spin polarization is negligible only at temperatures larger than ~ 1000 K and doping at the percent level, enforcing that spin-polarization should be

included in any study of larger graphene antidot lattices having zigzag edges. The increased band gap has a clear impact on the optical properties of GALs, demonstrating the importance of including this type of interaction when calculating physical observables such as optical response.

ACKNOWLEDGMENTS

T.G.P. gratefully acknowledges the financial support from the Center for Nanostructured Graphene (Project No. DNRFF58) financed by the Danish National Research Foundation. We thank J. G. Pedersen and A.-P. Jauho for useful comments on the manuscript.

*mlt@nano.aau.dk

¹K. S. Novoselov, V. I. Fal'ko, L. Colombo, P. R. Gellert, M. G. Schwab, and K. Kim, *Nature (London)* **490**, 192 (2012).

²A. S. Mayorov, R. V. Gorbachev, S. V. Morozov, L. Britnell, R. Jalil, L. A. Ponomarenko, P. Blake, K. S. Novoselov, K. Watanabe, T. Taniguchi, and A. K. Geim, *Nano Lett.* **11**, 2396 (2011).

³A. Reina, X. Jia, J. Ho, D. Nezich, H. Son, V. Bulovic, M. S. Dresselhaus, and J. Kong, *Nano Lett.* **9**, 30 (2009).

⁴B. Obradovic, R. Kotlyar, F. Heinz, P. Matagne, T. Rakshit, M. D. Giles, M. A. Stettler, and D. E. Nikonov, *Appl. Phys. Lett.* **88**, 142102 (2006).

⁵Y.-W. Son, M. L. Cohen, and S. G. Louie, *Phys. Rev. Lett.* **97**, 216803 (2006).

⁶S. Okada and A. Oshiyama, *Phys. Rev. Lett.* **87**, 146803 (2001).

⁷E. McCann, *Phys. Rev. B* **74**, 161403 (2006).

⁸Y. Zhang, T.-T. Tang, C. Girit, Z. Hao, M. C. Martin, A. Zettl, M. F. Crommie, Y. R. Shen, and F. Wang, *Nature (London)* **459**, 820 (2009).

⁹T. G. Pedersen, C. Flindt, J. Pedersen, N. A. Mortensen, A.-P. Jauho, and K. Pedersen, *Phys. Rev. Lett.* **100**, 136804 (2008).

¹⁰X. Liu, Z. Zhang, and W. Guo, *Small* **9**, 1405 (2013).

¹¹J. A. Fürst, J. G. Pedersen, C. Flindt, N. A. Mortensen, M. Brandbyge, T. G. Pedersen, and A.-P. Jauho, *New J. Phys.* **11**, 095020 (2009).

¹²R. Petersen and T. G. Pedersen, *Phys. Rev. B* **80**, 113404 (2009).

¹³R. Petersen, T. G. Pedersen, and A.-P. Jauho, *ACS Nano* **5**, 523 (2011).

¹⁴H. Y. He, Y. Zhang, and B. C. Pan, *J. Appl. Phys.* **107**, 114322 (2010).

¹⁵W. Liu, Z. F. Wang, Q. W. Shi, J. Yang, and F. Liu, *Phys. Rev. B* **80**, 233405 (2009).

¹⁶F. Ouyang, S. Peng, Z. Liu, and Z. Liu, *ACS Nano* **5**, 4023 (2011).

¹⁷D. Yu, E. M. Lupton, M. Liu, W. Liu, and F. Liu, *Nano Res.* **1**, 56 (2008).

¹⁸L. Chen, D. Yu, and F. Liu, *Appl. Phys. Lett.* **93**, 223106 (2008).

¹⁹H.-X. Yang, M. Chshiev, D. W. Boukhvalov, X. Waintal, and S. Roche, *Phys. Rev. B* **84**, 214404 (2011).

²⁰J. J. Palacios, J. Fernández-Rossier, and L. Brey, *Phys. Rev. B* **77**, 195428 (2008).

²¹T. G. Pedersen, C. Flindt, J. Pedersen, A.-P. Jauho, N. A. Mortensen, and K. Pedersen, *Phys. Rev. B* **77**, 245431 (2008).

²²T. G. Pedersen and J. G. Pedersen, *J. Appl. Phys.* **112**, 113715 (2012).

²³T. Gunst, T. Markussen, A.-P. Jauho, and M. Brandbyge, *Phys. Rev. B* **84**, 155449 (2011).

²⁴L. Rosales, M. Pacheco, Z. Barticevic, A. León, A. Latgé, and P. A. Orellana, *Phys. Rev. B* **80**, 073402 (2009).

²⁵Y.-T. Zhang, Q.-M. Li, Y.-C. Li, Y.-Y. Zhang, and F. Zhai, *J. Phys.: Condens. Matter* **22**, 315304 (2010).

²⁶H. Jippo, M. Ohfuchi, and C. Kaneta, *Phys. Rev. B* **84**, 075467 (2011).

²⁷C. Tao, L. Jiao, O. V. Yazyev, Y.-C. Chen, J. Feng, X. Zhang, R. B. Capaz, J. M. Tour, A. Zettl, S. G. Louie, H. Dai, and M. F. Crommie, *Nat. Phys.* **7**, 616 (2011).

²⁸O. V. Yazyev, R. B. Capaz, and S. G. Louie, *Phys. Rev. B* **84**, 115406 (2011).

²⁹J. Fernández-Rossier, *Phys. Rev. B* **77**, 075430 (2008).

³⁰S. R. Power, V. M. de Menezes, S. B. Fagan, and M. S. Ferreira, *Phys. Rev. B* **84**, 195431 (2011).

³¹M. Fujita, K. Wakabayashi, K. Nakada, and K. Kusakabe, *J. Phys. Soc. Jpn.* **65**, 1920 (1996).

³²S. Dutta and K. Wakabayashi, *Sci. Rep.* **2**, 519 (2012).

³³T. Hikihara, X. Hu, H.-H. Lin, and C.-Y. Mou, *Phys. Rev. B* **68**, 035432 (2003).

³⁴H. Feldner, Z. Y. Meng, T. C. Lang, F. F. Assaad, S. Wessel, and A. Honecker, *Phys. Rev. Lett.* **106**, 226401 (2011).

³⁵M. Golor, T. C. Lang, and S. Wessel, *Phys. Rev. B* **87**, 155441 (2013).

³⁶M. Kim, N. S. Safron, E. Han, M. S. Arnold, and P. Gopalan, *Nano Lett.* **10**, 1125 (2010).

³⁷J. Bai, X. Zhong, S. Jiang, Y. Huang, and X. Duan, *Nat. Nanotechnol.* **5**, 190 (2010).

³⁸M. Begliarbekov, O. Sul, J. Santanello, N. Ai, X. Zhang, E.-H. Yang, and S. Strauf, *Nano Lett.* **11**, 1254 (2011).

³⁹J. Eroms and D. Weiss, *New J. Phys.* **11**, 095021 (2009).

⁴⁰X. Jia, M. Hofmann, V. Meunier, B. G. Sumpter, J. Campos-Delgado, J. M. Romo-Herrera, H. Son, Y.-P. Hsieh, A. Reina, J. Kong, M. Terrones, and M. S. Dresselhaus, *Science* **323**, 1701 (2009).

⁴¹Ç. Ö. Girit, J. C. Meyer, R. Erni, M. D. Rossel, C. Kisielowski, L. Yang, C.-H. Park, M. F. Crommie, M. L. Cohen, S. G. Louie, and A. Zettl, *Science* **323**, 1705 (2009).

- ⁴²F. Oberhuber, S. Blien, S. Heydrich, F. Yaghobian, T. Korn, C. Schüller, C. Strunk, D. Weiss, and J. Eroms, *Appl. Phys. Lett.* **103**, 143111 (2013).
- ⁴³T. Shimizu, J. Nakamura, K. Tada, Y. Yagi, and J. Haruyama, *Appl. Phys. Lett.* **100**, 023104 (2012).
- ⁴⁴E. H. Lieb, *Phys. Rev. Lett.* **62**, 1201 (1989).
- ⁴⁵J. A. Furst, T. G. Pedersen, M. Brandbyge, and A.-P. Jauho, *Phys. Rev. B* **80**, 115117 (2009).
- ⁴⁶D. Sánchez-Portal, P. Ordejón, and E. Canadell, *Struct. Bond.* **113**, 103 (2004).
- ⁴⁷N. Troullier and J. L. Martins, *Phys. Rev. B* **43**, 1993 (1991).
- ⁴⁸J. P. Perdew and A. Zunger, *Phys. Rev. B* **23**, 5048 (1981).
- ⁴⁹Y. Hancock, A. Uppstu, K. Saloriotta, A. Harju, and M. J. Puska, *Phys. Rev. B* **81**, 245402 (2010).
- ⁵⁰M. Schüler, M. Rösner, T. O. Wehling, A. I. Lichtenstein, and M. I. Katsnelson, *Phys. Rev. Lett.* **111**, 036601 (2013).
- ⁵¹W. Zhu, G. Ding, and B. Dong, *Appl. Phys. Lett.* **100**, 103101 (2012).
- ⁵²N. D. Mermin and H. Wagner, *Phys. Rev. Lett.* **17**, 1133 (1966).
- ⁵³A. Gelfert and W. Nolting, *J. Phys.: Condens. Matter* **13**, R505 (2001).
- ⁵⁴D. K. Ghosh, *Phys. Rev. Lett.* **27**, 1584 (1971).
- ⁵⁵H. Lee, Y.-W. Son, N. Park, S. Han, and J. Yu, *Phys. Rev. B* **72**, 174431 (2005).
- ⁵⁶B.-L. Huang, M.-C. Chang, and C.-Y. Mou, *Phys. Rev. B* **82**, 155462 (2010).
- ⁵⁷B.-L. Huang and C.-Y. Mou, *Europhys. Lett.* **88**, 68005 (2009).
- ⁵⁸A. Lherbier, X. Blase, Y.-M. Niquet, F. Triozon, and S. Roche, *Phys. Rev. Lett.* **101**, 036808 (2008).
- ⁵⁹L. Ci, L. Song, C. Jin, D. Jariwala, D. Wu, Y. Li, A. Srivastava, Z. F. Wang, K. Storr, L. Balicas, F. Liu, and P. M. Ajayan, *Nat. Mater.* **7**, 430 (2010).